Molecular Structure of Kanamycin Nucleotidyltransferase Determined to 3.0-Å Resolution[†,‡]

Joshua Sakon,[§] Hans H. Liao,[∥] Agnes M. Kanikula,[∥] Matthew M. Benning,[§] Ivan Rayment,[§] and Hazel M. Holden*[,§]

Institute for Enzyme Research, Graduate School and Department of Biochemistry, and Biotechnology Center, University of Wisconsin, Madison, Wisconsin 53705

Received July 2, 1993; Revised Manuscript Received August 24, 1993[●]

ABSTRACT: Kanamycin nucleotidyltransferase, as originally isolated from *Staphylococcus aureus*, inactivates the antibiotic kanamycin by catalyzing the transfer of a nucleotidyl group from nucleoside triphosphates such as ATP to the 4′-hydroxyl group of the aminoglycoside. The molecular structure of the enzyme described here was determined by X-ray crystallographic analysis to a resolution of 3.0 Å. Crystals employed in the investigation belonged to the space group $P4_32_12$ with unit cell dimensions of $a = b = 78.9$ Å and $c = 219.2$ Å. An electron density map phased with seven heavy-atom derivatives revealed that the molecules packed in the crystalline lattice as dimers exhibiting local 2-fold rotation axes. Subsequent symmetry averaging and solvent flattening improved the quality of the electron density such that it was possible to completely trace the 253 amino acid polypeptide chain. Each monomer is divided into two distinct structural domains: the N-terminal motif composed of residues Met 1–Glu 127 and the C-terminal half delineated by residues Ala 128–Phe 253. The N-terminal region is characterized by a five-stranded mixed β-pleated sheet whereas the C-terminal domain contains five α-helices, four of which form an up-and-down α-helical bundle very similar to that observed in cytochrome *c′*. The two subunits wrap about one another to form an ellipsoid with a pronounced cleft that could easily accommodate the various aminoglycosides known to bind to the enzyme.

The aminoglycoside kanamycin belongs to a family of antibiotics consisting of one or more amino sugars connected to a basic aminocyclitol moiety by glycosidic bonds. Despite the introduction of newer, less toxic antimicrobial agents, these types of antibiotics continue to serve useful roles in the treatment of serious infections caused by a broad range of microorganisms including aerobic Gram-negative bacteria (Edson & Terrell, 1991; Johnson & Hardin, 1992). The bactericidal effect of aminoglycosides is most likely due to the irreversible binding of the drugs to the bacterial ribosomes (Moellering, 1983). Other mechanisms, such as disruption of the bacterial cytoplasmic membrane, have also been suggested to occur (Hancock, 1981; Tanaka, 1982; Bryan & Kwan, 1983; Taber *et al.*, 1987; Bryan, 1988). Due to the widespread usage of aminoglycosides, however, resistant bacterial strains have emerged, thereby markedly reducing the clinical effectiveness of such antibiotics. Resistance is conferred by the presence of plasmids, one of which encodes kanamycin nucleotidyltransferase (KNTase) (Le Goffic *et al.*, 1976a,b; Sadaie *et al.*, 1980).

KNTase, as originally isolated from *Staphylococcus aureus*, was shown to catalyze the transfer of a nucleoside monophosphate group from a nucleotide to the 4′-hydroxyl group of kanamycin (Le Goffic *et al.*, 1976a,b). The enzyme can utilize ATP, GTP, or UTP as the nucleoside monophosphate donor and can inactivate a wide range of aminoglycosides including kanamycins A, B, and C, gentamicin A, amikacin, tobramycin, and neomycins B and C (Davies & Smith, 1978; Le Goffic *et al.*, 1976b).

The amino acid sequence of KNTase is known from the nucleotide sequence (Matsumura *et al.*, 1984; Muller *et al.*, 1986; Bashkirov *et al.*, 1986). Each subunit contains 253 amino acid residues. Originally, KNTase was believed to be monomeric on the basis of nondenaturing gel electrophoresis (Sadaie *et al.*, 1980). The X-ray crystallographic studies described here, however, suggest that KNTase is a dimer with a local 2-fold rotational axis.

A model for the enzymatic mechanism of KNTase has not yet been fully established. It is possible, however, that KNTase operates by a mechanism similar to that of aminoglycoside nucleotidyltransferase 2″-I (Gates & Northrop, 1988a). Although KNTase and aminoglycoside nucleotidyltransferase 2″-I have little amino acid sequence homology, each enzyme transfers a nucleotide monophosphate group to an aminoglycoside, albeit to a different hydroxyl group (Gates & Northrop, 1988a). Aminoglycoside nucleotidyltransferase 2″-I obeys the Theorell–Chance kinetic mechanism in which nucleotide binding to the enzyme is followed by aminoglycoside binding. Subsequently, pyrophosphate is released followed by the nucleotidyl aminoglycoside. Enzyme turnover is controlled by the rate-limiting step of product release (Gates & Northrop, 1988b,c). In addition, studies have demonstrated inversion of the α-phosphate in the course of the reaction, indicating that the nucleoside monophosphate is directly transferred to the hydroxyl group of the antibiotic without an intermediate step (Van Pelt *et al.*, 1986).

Since KNTase is a relatively small, soluble protein that is easily purified and assayed and is selectable in a variety of bacterial species, it has proven in recent years to be an ideal system for the study of protein stability and folding. Ac-

[†] This research was supported in part by grants from the NIH (GM30982 and HL42322 to H.M.H. and GM351865 to I.R.) and from the Office of Naval Research (N00014-89-J-3134 to H.H.L.). H.M.H. is an Established Investigator of the American Heart Association.

[‡] X-ray coordinates for the α-carbon positions of the mutant KNTase have been deposited in the Brookhaven Protein Data Bank under the filename 1KAN (Bernstein *et al.*, 1977) or may be obtained immediately via HOLDEN@ENZYME.WISC.EDU.

* To whom correspondence should be addressed.

[§] Institute for Enzyme Research, Graduate School and Department of Biochemistry.

[∥] Biotechnology Center.

[●] Abstract published in *Advance ACS Abstracts,* October 15, 1993.

0006-2960/93/0432-11977$04.00/0

Table I: Intensity Statistics for the Native X-ray Data Set

		resolution range							
	overall	∞–8.46	–5.99	–4.90	–4.24	–3.79	–3.46	–3.21	–3.0
no. of measurements	70244	3887	9447	11819	12920	12187	9090	3984	3586
no. of independent reflections[a]	13914 (9534)	665 (507)	1227 (1112)	1558 (1459)	1844 (1743)	2020 (1844)	2152 (1569)	2205 (693)	2243 (607)
% of theoretical no. of reflections	95	87	98	100	100	98	96	94	96
av intensity		1468	407	482	613	424	293	179	96
σ		60	41	48	64	57	49	31	28
R-factor[b] (%)	7.5	2.4	5.2	6.7	7.1	9.4	11.7	12.8	20.9

[a] This is the number of reduced observations. Shown in parentheses is the number of independent measurements for which there were duplicate or symmetry-related observations. [b] R-factor = $\sum|I - \bar{I}|/\sum I \times 100$.

cordingly, the discovery of a thermostable KNTase, as isolated from the thermophile *Bacillus stearothermophilus*, that differed by only one amino acid (T130K) from that of the mesophile *S. aureus* has prompted a series of investigations to identify the cause of the thermostability (Hoshino *et al.*, 1985; Matsumura & Aiba, 1985; Matsumura *et al.*, 1986a,b, 1988; Liao *et al.*, 1986; Koizumi *et al.*, 1990; Liao, 1991). Another mutant, D80Y and T130K, has been prepared which shows catalytic activity at 70 °C (Matsumura & Aiba, 1985; Liao *et al.*, 1986) and has been crystallized in a form suitable for an X-ray analysis (Kanikula *et al.*, 1992). Here we describe the three-dimensional structure of this mutant determined to 3.0-Å resolution. The molecular architecture of KNTase is of special interest in that there are no reported three-dimensional structures for aminoglycoside-inactivating enzymes to date. Furthermore, the elucidation of the active site of KNTase will provide insight into the mechanism of nucleotide phosphate transfer and may provide a template for drug design.

EXPERIMENTAL PROCEDURES

Crystallization and Preparation of Heavy-Atom Derivatives. The KNTase mutant was expressed in an *Escherichia coli* overproducing strain BL21(DE3) carrying the expression plasmid pX(T7)TK101 (Studier & Moffatt, 1986; Liao, 1991). The enzyme purification scheme followed for this investigation was a modification of previously reported procedures and employed an initial chromatographic step with DEAE-Sephadex-6505, followed by HPLC steps with TSK phenyl-5PW and Mono-Q HR10/10 columns (Liao *et al.*, 1986; Liao, 1991; Sadaie *et al.*, 1980). The protein was stored in 10 mM Tris-HCl, pH 7.5 at –70 °C.

Two crystal forms of the enzyme were grown from poly(ethylene glycol) (PEG) 8000 solutions (Kanikula *et al.*, 1992). Type I crystals were obtained at 4 °C from solutions containing 19.0% (w/v) PEG 8000, 200 mM NaCl, 50 mM Hepes, pH 8.0, and 5 mM NaN_3. These crystals belonged to the space group $C222_1$ with unit cell dimensions of a = 128.4 Å, b = 156.8 Å, and c = 155.8 Å. Although the asymmetric unit contained four to six subunits, the crystals diffracted strongly to a nominal resolution of 2.4 Å. Type II crystals were grown at 4 °C by the hanging drop method of vapor diffusion against solutions containing 15.0% PEG 8000 and 50 mM Hepes, pH 8.0. The initial 20-μL protein droplets contained 4% PEG, 100 mM KCl, 25 mM Hepes, pH 8.0, 3 mM $CoCl_2$, and 2.5 mM NaN_3. The type II crystals belonged to the tetragonal space group $P4_32_12$ with unit cell dimensions of $a = b$ = 78.9 Å and c = 219.2 Å and two subunits per asymmetric unit. Due to the smaller asymmetric unit, the type II crystals were employed for the initial structural investigation reported here. However, these crystals do not diffract much beyond 2.8-Å resolution, and consequently, while they were important for obtaining an initial polypeptide chain tracing, further structural investigations directed toward understanding the interactions between KNTase, the nucleotide, and the aminoglycoside substrate will necessarily employ the type I crystals.

For heavy-atom derivative searches, the crystals were transferred to a synthetic mother liquor containing 15% PEG 8000, 400 mM KCl, 50 mM Hepes, pH 8.0, 6 mM $CoCl_2$, 5 mM NaN_3, and various heavy metal reagents. Seven isomorphous heavy-atom derivatives were prepared by soaking the crystals under the following conditions: (1) 0.5 mM K_2OsO_4 for 1 day, (2) 1 mM *cis*-$Pt(NH_2)_2Cl_2$ for 3 days, (3) 1 mM di-μ-iodobis(ethylenediamine)diplatinum(II) nitrate for 4 days, (4) 1 mM K_2PtCl_6 for 2 days, (5) 5 mM *p*-(hydroxymercuri)benzoate sodium salt for 5 days, (6) 20 mM trimethyllead acetate for 7 days, and (7) 20 mM triethyllead acetate for 4 days.

X-ray Data Collection and Processing. Crystals were mounted in thin-walled quartz capillary tubes and covered by a thin film of poly(vinylformal) dissolved in 1,2-dichloroethane to prevent crystal slippage in the X-ray beam (Rayment *et al.*, 1977). X-ray data from the native crystals and the seven heavy-atom derivatives were collected with a Siemens-Xentronics 1000 area detector system at 4 °C. These X-ray data were processed with the data reduction software package XDS (Kabsch, 1988a,b) and internally scaled according to the algorithm of Fox and Holmes (1966) as implemented by Dr. Phil Evans. The X-ray source was nickel-filtered Cu Kα radiation from a Rigaku RU200 rotating anode generator operated at 50 kV and 50 mA and equipped with a 200-μm focal cup. The native X-ray data set was 94% complete to 3.0-Å resolution, and relevant data collection statistics may be found in Table I.

Computational Methods. Each heavy-atom derivative X-ray data set was placed on the same scale as the native data by a "local" scaling procedure developed in the laboratory and described in Benning *et al.* (1992) and Rayment *et al.* (1992). The heavy-atom binding sites in the crystalline lattice were determined by the program HASSP and by visual inspection of appropriate difference Patterson maps calculated with X-ray data from 30.0 to 5.0 Å (Terwilliger *et al.*, 1987). These sites were placed on a common origin by difference Fourier maps. Positions, occupancies, and isotropic temperature factors for these heavy-atom binding sites were refined by the origin-removed Patterson-function correlation method as implemented in the program HEAVY (Rossmann, 1960; Terwilliger & Eisenberg, 1983). Protein phases were also calculated with HEAVY. These phases did not include information from the anomalous scattering of the heavy atoms. Relevant heavy-atom derivative and phase statistics may be found in Table II.

An electron density map, calculated to 5.0-Å resolution with centroid protein phases and a structure factor weighting scheme based on the figure of merit, was plotted onto

Table II: Relevant Heavy-Atom Derivative and Phase Statistics

compound	no. of binding sites	av isomorphous differences (%)[a]	resolution of data set (Å)	overall phasing power[b]	
				centric	acentric
K_2OsO_4	5	24	3.0	0.65	0.82
cis-$Pt(NH_2)_2Cl_2$	2	34	3.0	0.63	0.84
di-μ-iodobis(ethylenediamine)-diplatinum(II) nitrate	8	34	3.5	0.85	1.19
K_2PtCl_6	2	22	3.5	0.86	1.17
p-(hydroxymercuri)benzoate	6	30	3.0	0.87	1.14
trimethyllead acetate	3	33	3.0	0.76	0.98
triethyllead acetate	3	19	3.5	0.72	0.98

[a] $R = \sum||F_N| - |F_H||/\sum|F_N|$, where $|F_N|$ is the native structure factor amplitude and $|F_H|$ is the derivative structure factor amplitude. [b] Phasing power is the ratio of the root-mean-square heavy-atom scattering factor amplitude to the root-mean-square lack of closure error.

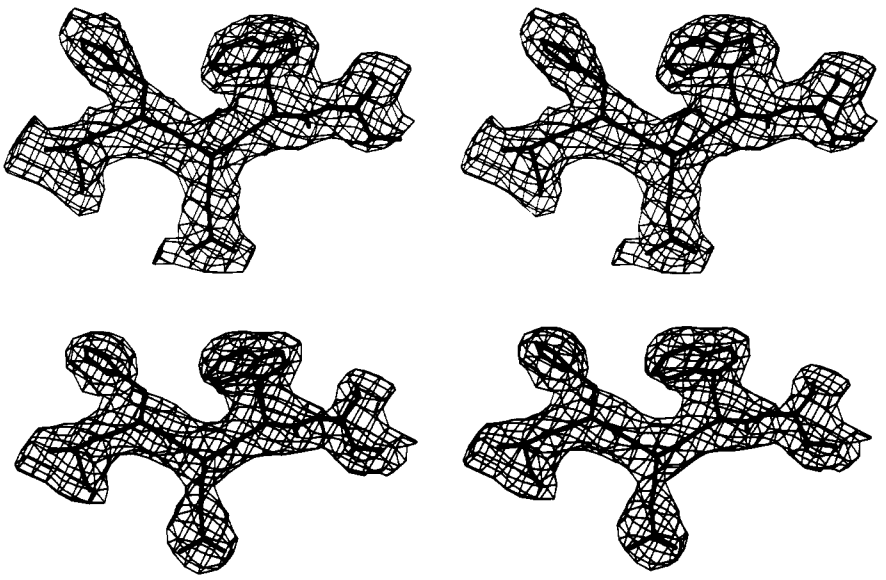

FIGURE 1: Representative portion of the electron density map calculated to 3.0-Å resolution. (a, top) A portion of the electron density corresponding to amino acid residues Ser 65–Thr 69 is shown. This stretch of β-sheet immediately follows a disordered surface loop. The electron density map, contoured at 1σ, was calculated by combining phases from seven heavy-atom derivatives and from noncrystallographic symmetry averaging and solvent flattening. (b, bottom) The same portion of the electron density map is shown but calculated with coefficients of the form $(2F_o - F_c)$, where F_o is the native structure factor amplitude and F_c is the calculated structure factor from the model refined at 3.0-Å resolution.

transparencies and stacked onto thin Plexiglas sheets. From this low-resolution map it was clear that the two molecules of KNTase had packed in the crystalline lattice as a dimer with a local 2-fold rotation axis, and thus it was possible to improve the quality of the protein phases by the techniques of molecular averaging and solvent flattening. This process was absolutely critical for solving the structure because the initial protein phases based on the heavy-atom derivatives alone were not good, as can be seen from the statistics presented in Table II.

The rotational matrix necessary for symmetry averaging was determined from the heavy-atom binding sites and optimized by the program MUNCHKINS (developed in the laboratory by Drs. G. Wesenberg and I. Rayment). A globally averaged electron density map to 5.0-Å resolution was then used to create a molecular envelope for subsequent refinement of the protein phases by iterative molecular averaging and solvent flattening according to the procedure of Bricogne (1976). The averaging was performed at 3.0-Å resolution for 15 cycles and yielded a final *R*-factor of 21.6% between the calculated structure factor amplitudes from the averaged electron density map and the observed X-ray data. In the resulting electron density map, the α-helices were left-handed, thus indicating that the initial choice of space group $P4_12_12$ was incorrect. The map was inverted to obtain the correct $P4_32_12$ unit cell.

The course of the polypeptide chain was traced with this averaged electron density map, the published cDNA sequence, and the molecular modeling program FRODO (Matsumura *et al.*, 1984; Muller *et al.*, 1986; Bashkirov *et al.*, 1986; Jones, 1985). Upon completion of the chain tracing, the "averaged" KNTase subunit was placed back into the unit cell and subjected to alternating cycles of least-squares refinement and manual model building with the program TNT (Tronrud *et al.*, 1987). To aid in the refinement process, protein phases based on the model were combined with the protein phases determined from the heavy-atom derivatives according to the algorithm of Dr. Randy J. Read (1986), who kindly supplied us with the software. These "combined" maps, along with electron density maps calculated with coefficients of the form $(2F_o-F_c)$, were employed in the rebuilding process. The present *R*-factor is 18.9% for all X-ray data between 30.0- and 3.0-Å resolution with root-mean-square deviations from "ideal" geometry of 0.012 for bond lengths, 3.0° for bond angles, and 0.009 Å for groups of atoms expected to be coplanar. No solvent molecules have been included in the refinement.

RESULTS AND DISCUSSION

Representative portions of the averaged electron density map used to build the KNTase model and the current map after least-squares refinement of the structure are presented in Figure 1. For the most part the polypeptide chain is well-

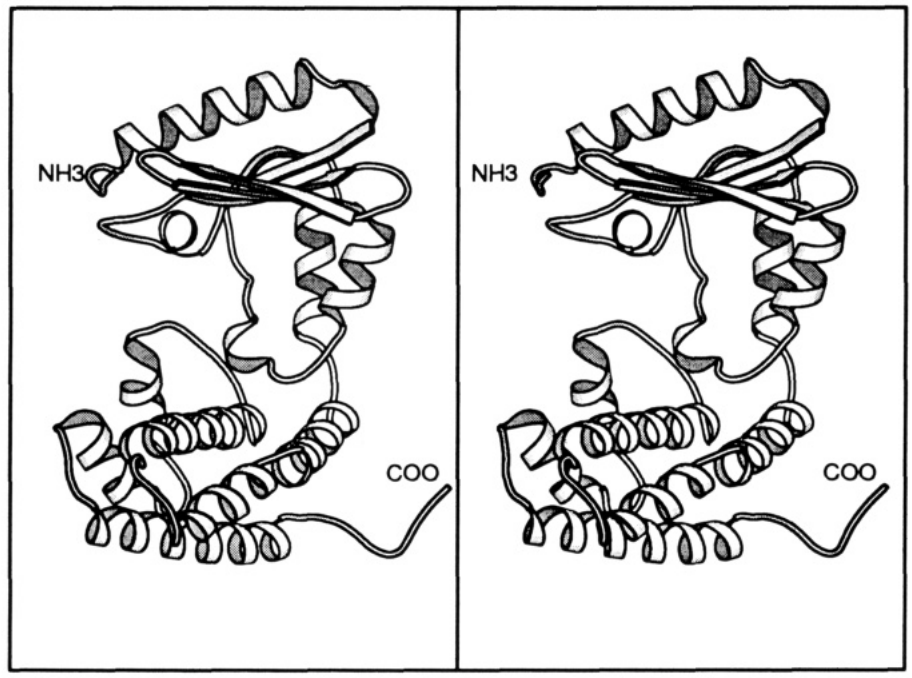

FIGURE 2: Ribbon representation of the KNTase subunit. This figure was prepared with the software package MOLSCRIPT (Kraulis, 1991).

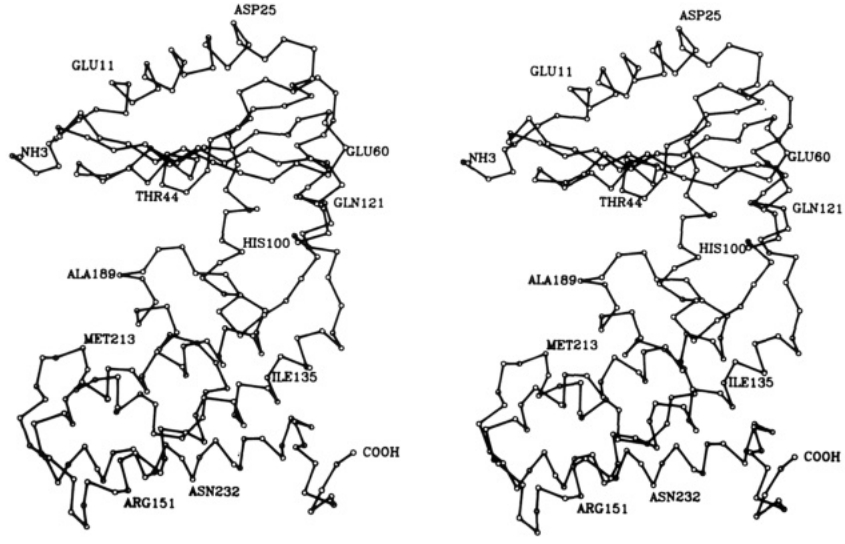

FIGURE 3: α-Carbon trace of the KNTase subunit. The molecule is shown in that same orientation as that in Figure 2. Amino acid residues are labeled at various positions along the polypeptide chain. This figure was generated with the software package PLUTO, originally developed by Dr. Sam Motherwell and modified for proteins by Eleanor Dodson and Phil Evans.

ordered except for the surface loops delineated by Tyr 27–Asp 30, Arg 42–Gly 46, and Glu 60–Ala 62. A ribbon representation and an α-carbon trace of the KNTase subunit may be found in Figures 2 and 3, respectively. The molecule is distinctly bilobal with the N-terminal domain built around a five-stranded mixed β-pleated sheet motif and four α-helices and the C-terminal region arranged predominantly in an up-and-down helical bundle. A list of the major secondary structural elements for the protein is given in Table III.

As can be seen in Figure 4, the topology of the β-sheet is such that strands 1 and 3 run in one direction whereas strands 2, 4, and 5 lie in the opposite direction. The so-called "P-loop", with the sequence Gly-Glu-Ser-Gly-Ala-Gly-Lys-Thr, as observed in myosin subfragment-1, adenylate kinase, and the Ras protein, is not present in KNTase (Walker *et al.*, 1982; Rayment *et al.*, 1993; Müller & Schulz, 1992; Pai *et al.*, 1990). The C-terminal domain of the enzyme falls into the classical category of up-and-down helical bundles as described by Richardson (1981). Other members in this category include, for example, myohemerythrin (Hendrickson & Ward, 1977), cytochrome b_{562} (Mathews *et al.*, 1972), cytochrome c' (Weber *et al.*, 1980), and apolipophorin-III (Breiter *et al.*, 1991). A superposition of the KNTase C-terminal domain with cytochrome c' may be found in Figure 5. Approximately 53% of the α-carbons for these two proteins superimpose with a root-mean-square deviation of 2.4 Å. The closest structural correspondence between cytochrome c' and

Table III: List of Secondary Structural Elements

amino acid residue no.	type of element	amino acid residue no.	type of element
9–25	α-helix	107–111	β-sheet
31–36	β-sheet	115–124	α-helix
39–42	α-helical turn	128–153	α-helix
51–57	β-sheet	162–180	α-helix
62–69	β-sheet	189–195	α-helix
74–81	β-sheet	205–214	α-helix
82–90	α-helix	220–241	α-helix
96–104	α-helix		

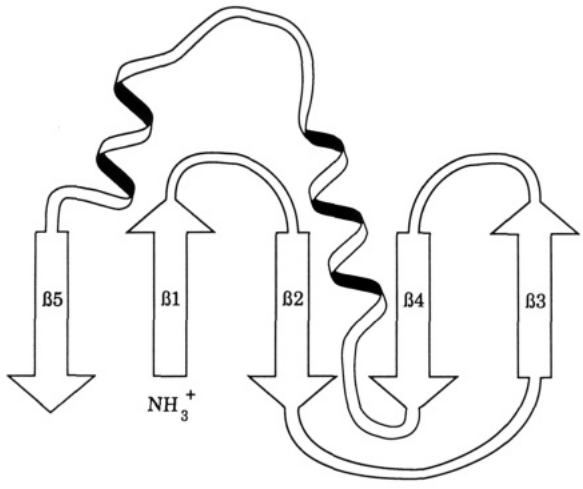

FIGURE 4: Topology of the KNTase β-sheet motif. This figure was provided by Dr. Bruce Jacobson, University of Wisconsin, Madison, WI. The two α-helices lie above the plane of the β-sheet.

KNTase occurs in the second helix where the two models superimpose with a root-mean-square value of 1.9 Å; the worst structural correspondence occurs in the third helix where the two proteins superimpose with a root-mean-square value of 3.3 Å. This third helix is distorted in KNTase.

KNTase was believed to function as a monomer (Sadaie, 1980). However, in the crystalline lattice, the two KNTase molecules clearly pack as a dimer with a 2-fold rotation axis running nearly parallel to the crystallographic *a*-axis. The α-carbon positions of the two KNTase subunits in the asymmetric unit superimpose with a root-mean-square deviation of 0.38 Å. A ribbon representation of the dimer is displayed in Figure 6. The two subunits are oriented in the dimer such that the C-terminal α-helical domain of one molecule fits into the cavity formed by the N- and C-terminal domains of the other. For the most part, the interface between the monomers is formed by electrostatic interactions. One region of contact occurs very near to the local symmetry axis where the loop defined by Gly 215–Ser 218 in subunit 1 interacts with the corresponding loop in subunit 2. Also, the last few C-terminal amino acid residues of one subunit wrap around the other monomer near its N-terminus. Specifically, the C-terminal carboxylate of subunit 1 is within hydrogen-bonding distance of the guanido group of Arg 22 in subunit

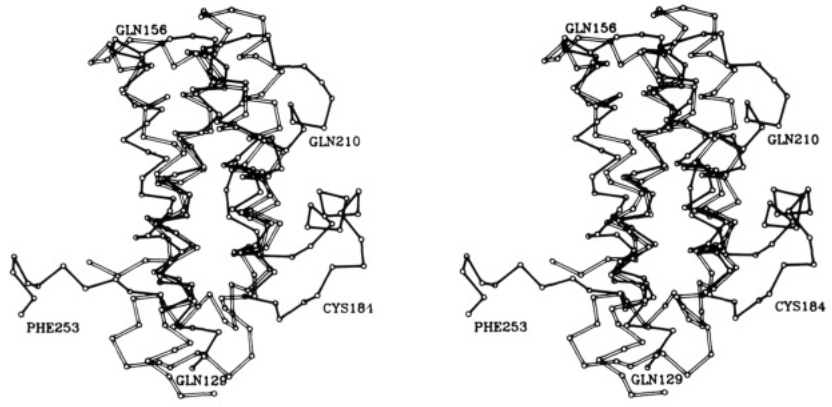

FIGURE 5: Comparison of the α-helical bundle in cytochrome *c'* and the C-terminal domain of KNTase. In this figure, cytochrome *c'* is displayed in open bonds while the C-terminal fragment of KNTase is depicted in solid bonds. The indicated amino acid residues correspond to the KNTase model. X-ray coordinates for cytochrome *c'* were determined by Weber *et al.* (1980) and obtained from the Brookhaven Protein Data Bank (Bernstein *et al.*, 1977).

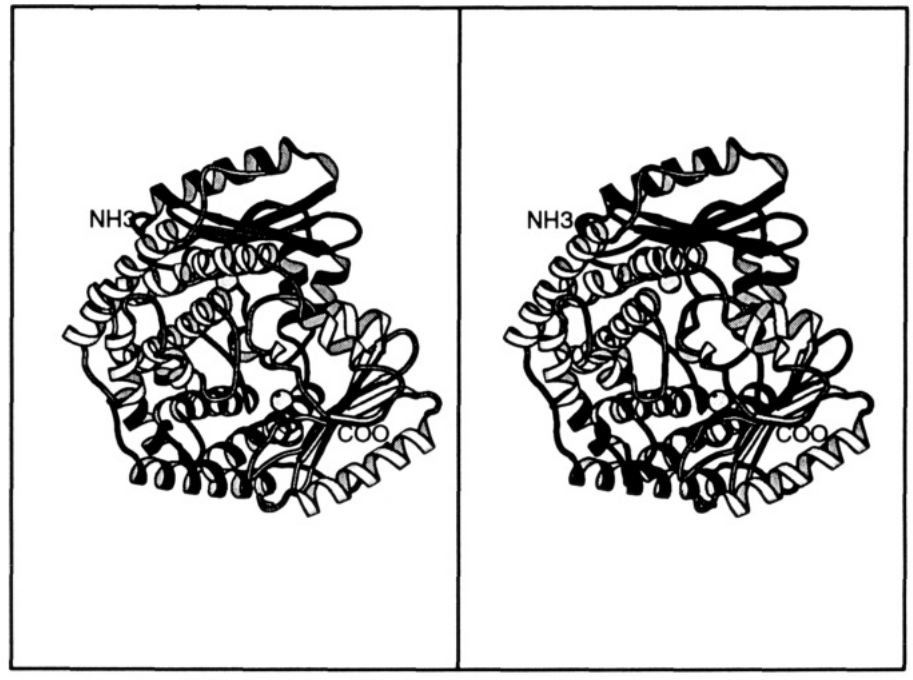

FIGURE 6: Ribbon representation of the KNTase dimer. The orientation of the dimer is such that the darkly shaded subunit 1 is in the same orientation as displayed in Figure 2. The lightly shaded subunit is positioned such that the C-terminal α-helical domain of subunit 1 fits into the pocket defined by the N- and C-terminal domains of subunit 2. The space-filling models represent the positions of the zinc binding sites.

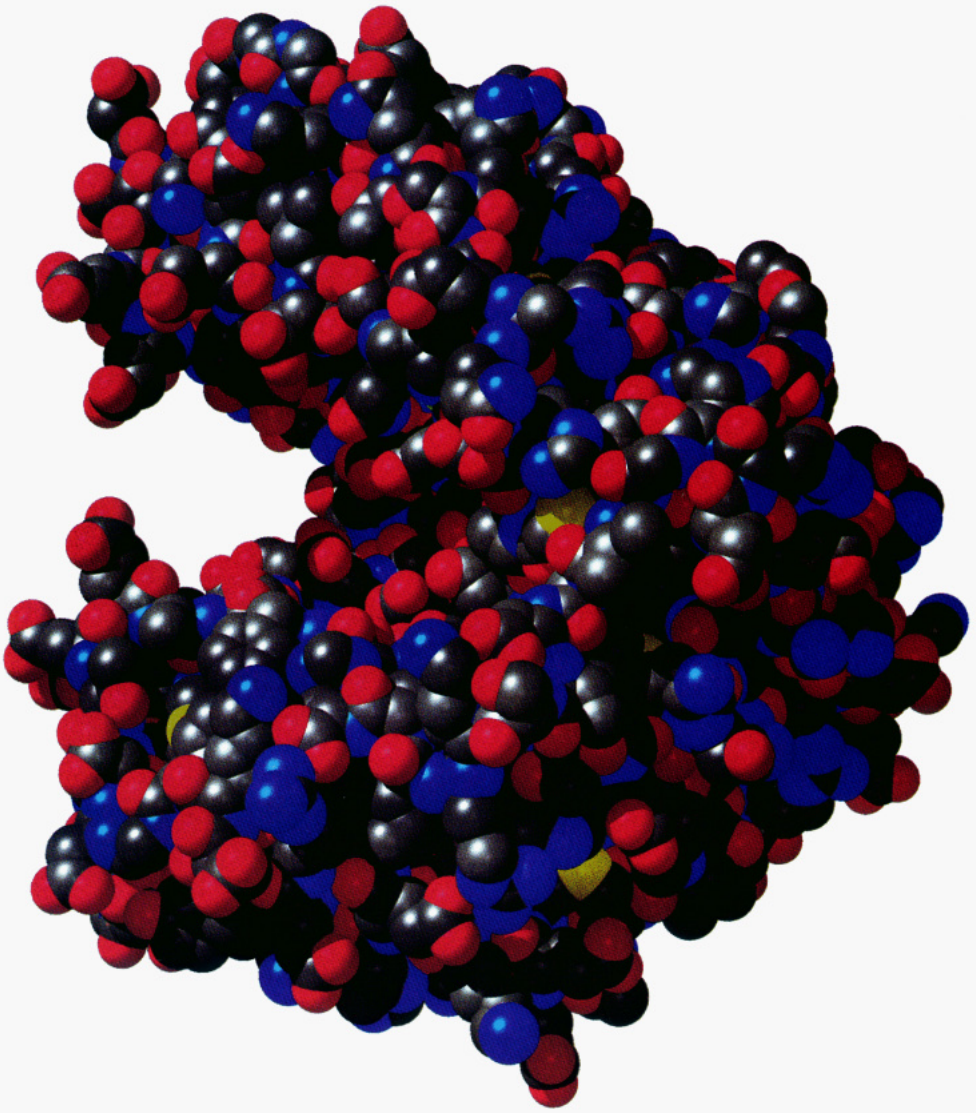

FIGURE 7: Space-filling representation of all atoms in the KNTase model. Oxygen, nitrogen, carbons, and sulfurs are depicted in red, blue, gray, and yellow, respectively. This figure was generated with the molecular graphics program MIDAS (Ferrin *et al.*, 1988).

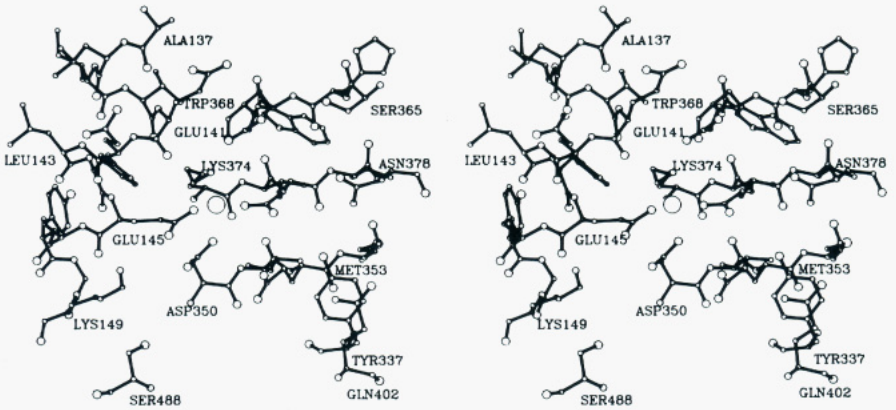

FIGURE 8: Close-up view of the putative zinc binding site. The zinc ion is shown as a large sphere in the middle of the figure. Those amino acid residues within approximately 10 Å of the zinc are displayed. Amino acid residue numbers less than 253 belong to subunit 1; those greater than 300 belong to subunit 2. The binding pocket, composed of residues from both subunits in the dimer, is flanked on the left by an α-helix (subunit 1) and on the right by three strands of β-sheet (subunit 2).

2. Also, the α-carbon of Met 1 in subunit 1 is 6 Å from the α-carbon of Gln 235 in subunit 2. By far, the most extensive region of protein–protein interactions occurs between the β-strand, reverse turn, β-strand motif of subunit 1 (Ala 62–Ser 81) and the α-helix (Ala 128–Ile 153) and C-terminus (Val 247–Pro 252) of subunit 2. This region constitutes the metal binding site as described below. From the space-filling representation in Figure 7, it can be seen that the two subunits form a basket with a very pronounced cleft. The overall dimensions of the dimer are 64 Å × 45 Å × 48 Å.

Preliminary atomic absorption experiments have indicated that KNTase binds Zn^{2+} ions (Liao, unpublished results). A difference Fourier map calculated to 3.0-Å resolution with coefficients of the form $(F_o - F_c)$ exhibited five significant peaks of electron density above 3σ. Two of these peaks, located within the interior of the KNTase dimer as displayed in Figure

6, are 22 Å apart and related by the molecular dyad. These peaks are too electron dense to be Mg^{2+} ions. Presumably they correspond to transition metals and are most likely either Co(II) or Zn(II) ions. For the KNTase model described here, they have been modeled into the electron density as zincs. A close-up view of the region within 10 Å of one of the putative zinc ions is given in Figure 8. The metal lies within bonding distance of the carboxylates contributed by Glu 76 of subunit 1 and Glu 145 of subunit 2. In the various zinc-containing enzyme structures determined thus far, the geometry about the metal is tetrahedral with typical ligands being cysteines and histidines. In the case of thermolysin and superoxide dismutase, one of the ligands is a glutamate or aspartate, respectively (Holmes & Matthews, 1982; Tainer *et al.*, 1982). The fact that tetrahedral coordination is not observed around the zinc in KNTase is undoubtedly due to the limits in the present resolution of the X-ray study for it is anticipated that solvent molecules or oxygens of the nucleotide substrates may also serve as ligands. The question of ligand geometry around the metal will be addressed in the structure determination of the type I crystals that is presently underway. The other three peaks observed in the difference Fourier map are located at crystalline contact regions and have been tentatively modeled into the electron density as Co^{2+} ions since the addition of $CoCl_2$ to the crystallization medium was critically important for obtaining the $P4_32_12$ crystal form. However, none of these metal ions are ligated in an octahedral configuration as would be expected for Co(II). Again, the exact coordination around these putative cobalt binding sites must await further structural studies at higher resolution.

As can be seen in Figure 8, there is a ring of seven negatively charged amino acid residues surrounding the zinc binding site (Glu 141, Glu 142, and Glu 145 from subunit 1 and Glu 52, Glu 67, Glu 76, and Asp 50 from subunit 2). This crown of amino acid residues further suggests that the region displayed in Figure 8 is, indeed, the active site since kanamycin and other aminoglycoside antibiotics are positively charged. It has been demonstrated that lanthanide ions form lanthanide–nucleotide complexes that can act as inhibitory analogs of Mg^{2+}-ATP (Morrison & Cleland, 1983). Consequently, soaking experiments with Lu^{3+}-ATP are presently underway in order to confirm the location of the KNTase active site.

The KNTase model described here is that of a thermostable double mutant, Asp 80–Tyr 80 and Thr 130–Lys 130. Tyr 80 is located at the end of the fourth strand of β-sheet whereas Lys 130 is positioned at the beginning of the fifth major α-helical region. These residues are not involved in intradomain interactions, in surface loops, in dimeric interfaces, or in crystalline contacts. Consequently, it is not obvious from the KNTase model why these mutations confer thermostability or why they allow crystallization of the mutant and not the native protein.

In summary, a model for the dimeric kanamycin nucleotidyltransferase has now been determined and refined to a resolution of 3.0 Å. Each subunit consists of two distinct domains, the N-terminal domain containing a five-stranded mixed β-pleated sheet and the C-terminal region consisting of an up-and-down α-helical bundle. The subunits associate around each other to form an ellipsoid with a deep cleft that contains two presumed zinc binding sites which are related to one another by the molecular dyad. The broad substrate specificity of KNTase may be partially explained by the presence of this large cleft. In addition, these zinc binding sites are surrounded by a series of negatively charged amino acid residues which may serve to orient the positively charged antibiotics. X-ray crystallographic experiments designed to determine protein–nucleotide–substrate interactions are presently underway.

REFERENCES

Bashkirov, V. I., Mil'shina, N. V., & Prozorov, A. A. (1986) *Genetika 22*, 1081–1092.

Benning, M. M., Smith, A. F., Wells, M. A., & Holden, H. M. (1992) *J. Mol. Biol. 228*, 208–219.

Bernstein, F. C., Koetzle, T. F., Williams, G. J. B., Meyer, E. F., Jr., Brice, M. D., Rogers, J. R., Kennard, O., Shimanouchi, T., & Tasumi, M. (1977) *J. Mol. Biol. 112*, 535–542.

Breiter, D. R., Kanost, M. R., Benning, M. M., Wesenberg, G., Law, J. H., Wells, M. A., Rayment, I., & Holden, H. M. (1991) *Biochemistry 30*, 603–608.

Bricogne, G. (1976) *Acta Crystallogr., Sect. A 32*, 832–847.

Bryan, L. E. (1988) *J. Antimicrob. Chemother. 22*, 1–15.

Bryan, L. E., & Kwan, S. (1983) *Antimicrob. Agents Chemother. 23*, 835–845.

Davies, J., & Smith, D. I. (1978) *Annu. Rev. Microbiol. 32*, 469–518.

Edson, R. S., & Terrell, C. L. (1991) *Mayo Clin. Proc. 66*, 1158–1164.

Ferrin, T. E., Langridge, R., Jarvis, L. E., & Huang, C. C. (1988) *J. Mol. Graphics 6*, 13–27.

Fox, G. C., & Holmes, K. C. (1966) *Acta Crystallogr. 20*, 886–891.

Gates, C. A., & Northrop, D. B. (1988a) *Biochemistry 27*, 3820–3825.

Gates, C. A., & Northrop, D. B. (1988b) *Biochemistry 27*, 3826–3833.

Gates, C. A., & Northrop, D. B. (1988c) *Biochemistry 27*, 3834–3842.

Hancock, R. E. W. (1981) *J. Antimicrob. Chemother. 8*, 249–276.

Hendrickson, W. A., & Ward, K. B. (1977) *J. Biol. Chem. 252*, 3012–3018.

Holmes, M. A., & Matthews, B. W. (1982) *J. Mol. Biol. 160* 623–639.

Hoshino, T., Ikeda, T., Furukawa, K., & Tomizuka, N. (1985) *Can. J. Microbiol. 31*, 614–619.

Johnson, J. G., & Hardin, T. C. (1992) *Clin. Podiatr. Med. Surg. 9*, 443–464.

Jones, A. T. (1985) *Methods Enzymol. 115*, 157–171.

Kabsch, W. (1988a) *J. Appl. Crystallogr. 21*, 67–71.

Kabsch, W. (1988b) *J. Appl. Crystallogr. 21*, 916–924.

Kanikula, A. M., Liao, H. H., Sakon, J., Holden, H. M., & Rayment, I. (1992) *Arch. Biochem. Biophys. 295*, 1–4.

Koizumi, J.-I., Zhang, M., Imanaka, T., & Aiba, S. (1990) *Appl. Environ. Microbiol. 56*, 3612–3614.

Kraulis, P. J. (1991) *J. Appl. Crystallogr. 24*, 946–950.

Le Goffic, F., Baca, B., Soussy, Cl. J., Dublanchet, A., & Duval, J. (1976a) *Ann. Microbiol. 127A*, 391–399.

Le Goffic, F., Martel, A., Capmau, M. L., Baca, B., Goebel, P., Chardon, H., Soussy, C. J., Duval, J., & Bouanchaud, D. H. (1976b) *Antimicrob. Agents Chemother. 10*, 258–264.

Liao, H. (1991) *Protein Expression Purif. 2*, 43–50.

Liao, H., McKenzie, T., & Hageman, R. (1986) *Proc. Natl. Acad. Sci. U.S.A. 83*, 576–580.

Mathews, F. S., Levine, M., & Argos, P. (1972) *J. Mol. Biol. 64*, 449–464.

Matsumura, M., & Aiba, S. (1985) *J. Biol. Chem. 260*, 15298–15303.

Matsumura, M., Katakura, Y., Imanaka, T., & Aiba, S. (1984) *J. Bacteriol. 160*, 413–420.

Matsumura, M., Kataoka, S., & Aiba, S. (1986a) *Mol. Gen. Genet. 204*, 355–358.

Matsumura, M., Yasumura, S., & Aiba, S. (1986b) *Nature 323*, 356–358.

Matsumura, M., Yahanda, S., Yasumura, S., Yutani, K. & Aiba, S. (1988) *Eur. J. Biochem. 171*, 715–720.

Moellering, R. C., Jr. (1983) *Rev. Infect. Dis. 5*, S212–S232.

Morrison, J. F., & Cleland, W. W. (1980) *Biochemistry 19*, 3127–3131.
Müller, C. W., & Schulz, G. E. (1992) *J. Mol. Biol. 224*, 159–177.
Muller, R. E., Ano, T., Imanaka, T., & Aiba, S. (1986) *Mol. Gen. Genet. 202*, 169–171.
Pai, E. F., Krengel, U., Petsko, G. A., Goody, R. S., Kabsch, W., & Wittinghofer, A. (1990) *EMBO J. 9*, 2351–2359.
Rayment, I., Johnson, J. E., & Suck, D. (1977) *J. Appl. Crystallogr. 19*, 365.
Rayment, I., Wesenberg, G., Meyer, T. E., Cusanovich, M. A., & Holden, H. M. (1992) *J. Mol. Biol. 228*, 672–686.
Rayment, I., Rypniewski, W. R., Schmidt-Bäse, K., Smith, R., Tomchick, D. R., Benning, M. M., Winkelmann, D. A., Wesenberg, G., & Holden, H. M. (1993) *Science* (in press).
Read, R. J. (1986) *Acta Crystallogr., Sect. A 42*, 140–149.
Richardson, J. (1981) *Adv. Protein Chem. 34*, 167–339.
Rossmann, M. G. (1960) *Acta Crystallogr. 13*, 221–226.
Sadaie, Y., Burtis, K. C., & Doi, R. H. (1980) *J. Bacteriol. 141*, 1178–1182.
Studier, F. W., & Moffatt, B. A. (1986) *J. Mol. Biol. 189*, 113–130.
Taber, H. W., Mueller, J. P., Miller, P. F., & Arrow, A. S. (1987) *Microbiol. Rev.*, 439–457.
Tainer, J. A., Getzoff, E. D. Beem, K. M. Richardson, J. S., & Richardson, D. C. (1982) *J. Mol. Biol. 160*, 181–217.
Tanaka, N. (1982) in *Handbook of Experimental Pharmacology* (Muezawa, H., & Hooper, I. R., Eds.) Vol. 62, pp 221–266, Springer-Verlag, New York.
Terwilliger, T. C., & Eisenberg, D. (1983) *Acta Crystallogr., Sect. A 39*, 813–817.
Terwilliger, T. C., Kim, S.-H., & Eisenberg, D. (1987) *Acta Crystallogr., Sect. A 43*, 1–5.
Tronrud, D. E., Ten Eyck, L. F., & Matthews, B. W. (1987) *Acta Crystallogr., Sect. A 43*, 489–501.
Van Pelt, J. E., Iyengar, R., & Frey, P. (1986) *J. Biol. Chem. 261*, 15995–15999.
Walker, J. E., Saraste, M., Runswick, M. J., & Gay, N. J. (1982) *EMBO J. 1*, 945–951.
Weber, P. C., Bartsch, R. G., Cusanovich, M. A., Hamlin, R. C., Howard, A., Jordon, S. R., Kamen, M. D., Meyer, T. E., Weatherford, D. W., Xuong, N. H., & Salemme, F. R. (1980) *Nature 286*, 302–304.